Photometric Redshift Requirements for Self-Calibration of Cluster Dark Energy Studies

Marcos Lima[1,2] and Wayne Hu[2,3*]
[1] *Department of Physics, University of Chicago, Chicago IL 60637*
[2] *Kavli Institute for Cosmological Physics, University of Chicago, Chicago IL 60637*
[3] *Department of Astronomy & Astrophysics and Enrico Fermi Institute, University of Chicago, Chicago IL 60637*
(Dated: September 18, 2007)

The ability to constrain dark energy from the evolution of galaxy cluster counts is limited by the imperfect knowledge of cluster redshifts. Ongoing and upcoming surveys will mostly rely on redshifts estimated from broad-band photometry (photo-z's). For a Gaussian distribution for the cluster photo-z errors and a high cluster yield cosmology defined by the WMAP 1 year results, the photo-z bias and scatter needs to be known better than 0.003 and 0.03, respectively, in order not to degrade dark energy constrains by more than 10% for a survey with specifications similar to the South Pole Telescope. Smaller surveys and cosmologies with lower cluster yields produce weaker photo-z requirements, though relative to worse baseline constraints. Comparable photo-z requirements are necessary in order to employ self-calibration techniques when solving for dark energy and observable-mass parameters simultaneously. On the other hand, self-calibration in combination with external mass inferences helps reduce photo-z requirements and provides important consistency checks for future cluster surveys. In our fiducial model, training sets with spectroscopic redshifts for $\sim 5\% - 15\%$ of the detected clusters are required in order to keep degradations in the dark energy equation of state lower than 20%.

I. INTRODUCTION

The abundance of clusters of galaxies as a function of their mass and redshift is potentially a powerful cosmological probe. The sensitivity to the underlying cosmology comes from the dependence of the abundance on the comoving volume element and, more importantly, from the exponential sensitivity of the cluster mass function to the amplitude of linear density perturbations. Both of these features depend upon the matter content of the universe and the underlying theory of gravity. Possible applications include constraints on theories of modified gravity [1], neutrino masses [2], the total matter density Ω_M and the amplitude of linear fluctuations σ_8 [3, 4]. Furthermore, cluster counts as a function of redshift offer a promising technique to explore and constrain dark energy parameters because of the suppression in the growth of perturbations during the acceleration epoch. In practice these studies are done by comparing observations to theoretical predictions from simulations as a function of cosmology.

However, there are many observational challenges to the use of clusters to constrain cosmology. First, there are different techniques of cluster detection, each one attempting to obtain cluster samples as complete and clean as possible. Typical cluster finding methods explore signals such as the Sunyaev-Zel'dovich (SZ) flux decrement, X-ray temperature, X-ray surface brightness, overdensities in space and color from optical observations and the weak lensing shear. When comparing the properties of the observed samples to simulation predictions, knowledge of the selection function is essential since observational effects particular to each cluster finder need to be properly accounted for.

Next, cluster masses must be estimated in ways that may or may not be tied to the cluster finder employed. In general, the mass is not a direct observable and needs to be obtained through the relation between an observable proxy and mass, the observable-mass relation. Uncertainties in mass conversion can lead to degenerate effects that destroy most of the information in cluster counts if not well calibrated.

In order to overcome this degeneracy a set of so-called self-calibration techniques has been developed recently. By requiring consistency between number counts and other cluster properties, it is possible to solve simultaneously for cosmology and observable-mass parameters. This can be accomplished by follow-up of a small cluster sample [5], by using information on the clustering properties of clusters from their power spectrum [5] or their sample covariance from counts in cells [6, 7], and by using information from the shape of the observed mass function [7, 8]. Another approach uses physical models of cluster structure [9] which is similar in spirit to imposing priors on observable-mass parameters. Combining these approaches allows for tests of the assumptions underlying the individual approaches.

Finally, cluster redshifts must be estimated. Whereas spectroscopic redshifts are very accurate, when dealing with large data sets it becomes impractical to obtain spectra for large fractions of objects. Alternatively redshifts can be estimated from broad-band photometry in a finite number of filter band-passes (see e.g. [10] and references therein). Photometry can be viewed as a coarse spectroscopy that probes the most prominent spectral features as they move from their rest positions when the

*Electronic address: mvlima@uchicago.edu

object of interest is redshifted. Redshifts thus estimated, known as photometric redshifts (photo-z's), can be efficiently calculated for millions of objects and can use not only colors but any observable that correlates with redshift [11].

Since the interpretation of the counts depends sensitively on an accurate determination of the redshift distribution of the clusters and not on the redshift precision for an individual cluster, photo-z's are well suited to such studies. Clusters detected by the SZ effect, for instance, will typically be followed up optically so that photo-z's can be calculated. Optical cluster finding algorithms can choose to derive photo-z's during the cluster finding process itself [12, 13] or use externally derived photo-z's [14, 15] with different implications for the propagation of photo-z errors.

In this paper, we study how the knowledge of the cluster photo-z error distribution can affect the ability to use cluster counts to constrain dark energy. Previous works have addressed this question for different cosmological probes, including cluster counts [16], supernova [16], baryon acoustic oscillations [17, 18] and weak lensing tomography [19, 20]. In particular, Huterer et al. [16] studied the effect of systematic shifts in centroids of redshift bins on cosmological constraints, in the context of perfect knowledge of cluster masses. Here we generalize that analysis by considering the full redshift error distribution and allowing redshift bias and scatter parameters to be arbitrary functions of redshift. We also consider the photo-z requirements necessary for self-calibration of the observable-mass relation when one is simultaneously solving for cluster masses and cosmology.

We start in §II and §III describing how redshift errors affect cluster number counts and their sample covariance respectively. In §IV we describe the fiducial models assumed and the Fisher matrix formalism, which is employed in §V to study how redshift errors degrade dark energy constraints in various cases of interest. Finally, in §VI we discuss the results and conclude.

II. NUMBER COUNTS

For a given cosmology, simulations predict the comoving number density of dark matter halos as a function of mass and redshift. For illustrative purposes, we will identify these halos with clusters and employ a fit to simulations for the halo differential comoving number density [21]

$$\frac{d\bar{n}}{d\ln M} = 0.3\frac{\rho_m}{M}\frac{d\ln\sigma^{-1}}{d\ln M}\exp[-|\ln\sigma^{-1}+0.64|^{3.82}]\,, \quad (1)$$

where $\sigma^2(M;z)\equiv\sigma_R^2(z)$, the linear density field variance in a region enclosing $M=4\pi R^3\rho_m/3$ at the mean matter density today ρ_m. Because shifts in cluster masses can modify cluster counts mimicking a change in cosmology, the exponential sensitivity to σ will only be a benefit in practice if the observable-mass distribution is also well known. Fortunately observations and simulations suggest observable-mass scaling relations that can be parametrized in simple forms and allow for reasonable degree of calibration [22, 23, 24]. Following [7], we take the probability of assigning a mass $M^{\rm obs}$ to a cluster of true mass M to be given by a Gaussian distribution in $\ln M$

$$p(M^{\rm obs}|M) = \frac{1}{\sqrt{2\pi\sigma^2_{\ln M}}}\exp\left[-x^2(M^{\rm obs})\right]\,, \quad (2)$$

where

$$x(M^{\rm obs}) \equiv \frac{\ln M^{\rm obs}-\ln M-\ln M^{\rm bias}}{\sqrt{2\sigma^2_{\ln M}}}\,. \quad (3)$$

For simplicity, we will allow the mass bias $\ln M^{\rm bias}$ and the variance $\sigma^2_{\ln M}$ to vary with redshift but not mass. The redshift dependent average number density of clusters within the observable mass range $M^{\rm obs}_\alpha \le M^{\rm obs} \le M^{\rm obs}_{\alpha+1}$ is given by

$$\begin{aligned}\bar{n}_\alpha(z) &\equiv \int_{M^{\rm obs}_\alpha}^{M^{\rm obs}_{\alpha+1}}\frac{dM^{\rm obs}}{M^{\rm obs}}\int\frac{dM}{M}\frac{d\bar{n}}{d\ln M}p(M^{\rm obs}|M)\\ &= \int\frac{dM}{M}\frac{d\bar{n}}{d\ln M}\frac{1}{2}\left[{\rm erfc}(x_\alpha)-{\rm erfc}(x_{\alpha+1})\right]\,, \quad (4)\end{aligned}$$

where $x_\alpha = x(M^{\rm obs}_\alpha)$. Notice that this corresponds to the cumulative number density above some sharp mass threshold in the limit that $\sigma^2_{\ln M}\to 0$ and $M^{\rm obs}_{\alpha+1}\to\infty$. The mean number of clusters is then obtained by integrating the mean number density in the redshift dependent comoving volume element d^3x. Let us use spherical coordinates to parametrize the spatial position vector as $\mathbf{x}=(r,\theta,\phi)$, where $r(z)$ is the angular diameter distance to redshift z and (θ,ϕ) parametrize the solid angle Ω such that $d\Omega=\sin\theta d\theta d\phi$. Since we will only consider flat cosmologies, $r(z)$ coincides with the comoving distance. The volume element is given by

$$d^3x = r^2 dr d\Omega = \frac{r^2(z)}{H(z)}dz d\Omega\,, \quad (5)$$

where $H(z)$ is the Hubble parameter to redshift z. Redshift uncertainties affect the redshift bin size as well as the observed angle, distorting the volume element and changing the number counts. We take the probability of assigning a photo-z $z^{\rm phot}$ to a cluster of true redshift z to be also a Gaussian distribution

$$p(z^{\rm phot}|z) \;=\; \frac{1}{\sqrt{2\pi\sigma_z^2}}\exp\left[-y^2(z^{\rm phot})\right]\,, \quad (6)$$

where

$$y(z^{\rm phot}) \;\equiv\; \frac{z^{\rm phot}-z-z^{\rm bias}}{\sqrt{2\sigma_z^2}} \quad (7)$$

and the redshift bias $z^{\rm bias}=z^{\rm bias}(z)$ and variance $\sigma_z^2=\sigma_z^2(z)$ are allowed to be arbitrary functions of redshift.

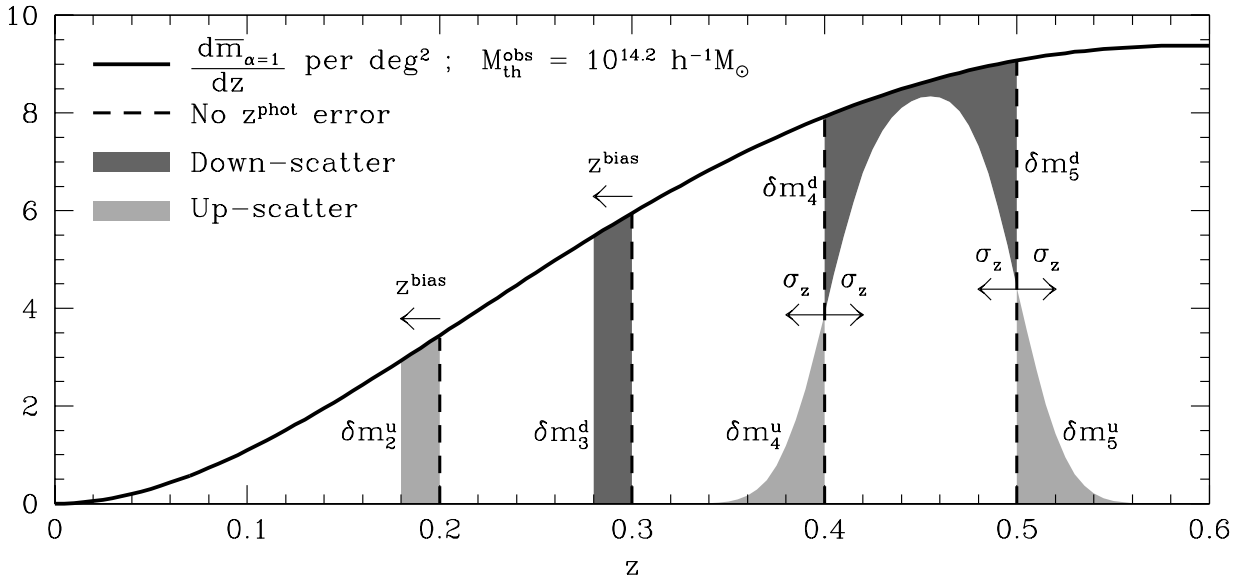

FIG. 1: The redshift distribution of cluster counts per deg^2 above a sharp mass threshold $M_{\rm th}^{\rm obs} = 10^{14.2}h^{-1}M_\odot$ is shown (solid line) for the fiducial survey properties defined in §IV in the WMAP1 cosmology. The effects of photo-z bias and scatter are shown for $z^{\rm bias} = \sigma_z = 0.02$ at redshift bins $[0.2, 0.3]$ and $[0.4, 0.5]$ respectively. The dashed lines indicate a perfect redshift selection in the absence of photo-z uncertainties. Photo-z errors scatter objects up (light gray) and down (dark gray), changing the observed number counts. In the limit that $\sigma_z^2 \to 0$, a positive redshift bias decreases counts in regions where dm/dz is increasing and vice-versa; the sensitivity of the counts is then controlled by $-d^2m/dz^2$ at the bin. The effect of scatter in each bin border scales as $\sim 0.5d^2m/dz^2$ in this limit; the total effect then depends on how d^2m/dz^2 varies from bin to bin and is proportional to $0.5d^3m/dz^3$.

Given a perfect angular selection characterized by an angular top hat window $W_i^{\rm th}(\Omega)$, the mean number of clusters in a photo-z bin defined by $z_i^{\rm phot} \le z^{\rm phot} \le z_{i+1}^{\rm phot}$ is

$$\begin{aligned}\bar{m}_{\alpha,i} &= \int_{z_i^{\rm phot}}^{z_{i+1}^{\rm phot}} dz^{\rm phot} \int d^3x \bar{n}_\alpha W_i^{\rm th}(\Omega) p(z^{\rm phot}|z) \\ &= \int d^3x \bar{n}_\alpha W_i(\mathbf{x})\,, \end{aligned} \tag{8}$$

where the total window function $W_i(\mathbf{x})$ is given by

$$W_i(\mathbf{x}) = W_i^{\rm th}(\Omega) F_i(z)\,, \tag{9}$$

and

$$\begin{aligned} F_i(z) &= \int_{z_i^{\rm phot}}^{z_{i+1}^{\rm phot}} dz^{\rm phot} p(z^{\rm phot}|z) \\ &= \frac{1}{2}\left[{\rm erfc}(y_i) - {\rm erfc}(y_{i+1})\right]\,, \end{aligned} \tag{10}$$

with $y_i = y(z_i^{\rm phot})$. The total window function in Eq. (9) takes into account photo-z error information carried by $F_i(z)$. Notice that when $z^{\rm bias} = \sigma_z = 0$, the distribution $p(z^{\rm phot}|z) = \delta(z^{\rm phot} - z)$ and $F_i(z)$ becomes a top hat $W_i^{\rm th}(z)$, which combined with the angular top hat produces the full 3d top hat window $W_i^{\rm th}(\mathbf{x}) = W_i^{\rm th}(\Omega)W_i^{\rm th}(z)$ of a perfect selection. Using Eqs. (5), (8), (9) and (10) the mean number counts in a cell defined by the photo-z bin and a solid angle $\Delta\Omega$ can be written as

$$\begin{aligned}\bar{m}_{\alpha,i} &= \int d\Omega dz \frac{r^2(z)}{H(z)} \bar{n}_\alpha(z) W_i^{\rm th}(\Omega) F_i(z) \\ &= \int dz \frac{d\bar{m}_\alpha}{dz} \frac{1}{2}\left[{\rm erfc}(y_i) - {\rm erfc}(y_{i+1})\right]\,, \end{aligned} \tag{11}$$

where we used the angular top hat window to perform the solid angle integral and defined

$$\frac{d\bar{m}_\alpha}{dz} \equiv \Delta\Omega \frac{r^2(z)\bar{n}_\alpha(z)}{H(z)}\,. \tag{12}$$

The solid angle $\Delta\Omega$ is related to the angular extension θ_s of the cell by

$$\Delta\Omega = \int d\Omega W_i^{\rm th}(\Omega) = 2\pi(1 - \cos\theta_s) \approx \pi\theta_s^2 \tag{13}$$

and the approximation is true in the flat sky regime, valid for small angle windows.

It is instructive to consider the sensitivity of number counts to the photo-z parameters in some limits. Let us consider the simple case of a sharp mass threshold (i.e. drop the $\alpha = 1$ index) and let us assume that the redshift bias and variance are smooth functions of redshift. From Eq. (11), the relative sensitivity of the mean counts $\bar{m}_i = \bar{m}_{\alpha=1,i}$ in a photo-z bin of width $\delta z_i^p = z_{i+1}^{\rm phot} - z_i^{\rm phot}$ to

the redshift bias around $\sigma_z^2 = 0$ is

$$\lim_{\sigma_z^2\to 0}\frac{\partial \ln \bar{m}_i}{\partial z^{\rm bias}} = \frac{1}{\bar{m}_i}\frac{d\bar{m}}{dz}\Big|_{y_{i+1}=0}^{y_i=0} \sim -\frac{1}{\bar{m}_i}\frac{d^2\bar{m}}{dz^2}\delta z_i^p\,, \quad (14)$$

whereas the sensitivity to the redshift variance is

$$\lim_{\sigma_z^2\to 0}\frac{\partial \ln \bar{m}_i}{\partial \sigma_z^2} = -\frac{1}{2\bar{m}_i}\frac{d^2\bar{m}}{dz^2}\Big|_{y_{i+1}=0}^{y_i=0} \sim \frac{1}{2\bar{m}_i}\frac{d^3\bar{m}}{dz^3}\delta z_i^p\,, (15)$$

and the derivatives are evaluated at the photo-z bin center $z_i^p = (z_i^{\rm phot}+z_{i+1}^{\rm phot})/2$. Note that these derivatives are insensitive to the actual value of σ_z^2 in this limit. Consequently we will employ the variance σ_z^2 instead of the rms σ_z in the forecasts below.

In general, the sensitivity of the counts to higher moments of the photo-z error distribution will depend on higher derivatives of the true redshift distribution and will tend to be less important. Fig. 1 shows the redshift distribution given by Eq. (12) plotted as a function of redshift for the fiducial model defined in § IV as well as the effects of $z^{\rm bias}$ and σ_z on the observed number counts. The distribution is shown only up to $z = 0.6$ for clarity.

The result of Eq. (14) is intuitive from the fact that a positive redshift bias decreases the counts in regions where the redshift distribution is increasing and vice-versa. Consider the effect of the redshift bias on the number counts in the redshift bin $[z_2, z_3] = [0.2, 0.3]$ as shown in Fig. 1. We have that $\partial\bar{m}_2/\partial z^{\rm bias} \sim (\delta m_2^u - \delta m_3^d)/z^{\rm bias}$, where δm_2^u is number of upscattered clusters around z_2 and δm_3^d is the number of downscattered clusters around z_3. Approximating these by rectangles, we can combine

$$\delta m_2^u \sim \frac{d\bar{m}}{dz}\Big|^{z_2} z^{\rm bias}\,, \quad (16)$$

with a similar expression for δm_3^d, and obtain Eq. (14).

The sensitivity to the redshift variance allows a similar interpretation. In Fig. 1 we consider the effect of the redshift scatter on the counts in the redshift bin $[z_4, z_5] = [0.4, 0.5]$. In this case we have $\partial\bar{m}_4/\partial\sigma_z^2 \sim (\delta m_4^u - \delta m_4^d + \delta m_5^u - \delta m_5^d)/\sigma_z^2$. Approximating these now by triangles, we have

$$\delta m_4^u \sim \frac{1}{2}\left[0.5\frac{d\bar{m}}{dz}\Big|^{z_4-\sigma_z}\right]\sigma_z\,. \quad (17)$$

A similar expression for δm_4^d at $z_4 + \sigma_z$ gives

$$\frac{(\delta m_4^u - \delta m_4^d)}{\sigma_z^2} \sim \frac{0.5}{2\sigma_z}\frac{d\bar{m}}{dz}\Big|_{z_4+\sigma_z}^{z_4-\sigma_z} \sim -0.5\frac{d^2\bar{m}}{dz^2}\Big|^{z_4}. \quad (18)$$

The corresponding result for $(\delta m_5^u - \delta m_5^d)/\sigma_z^2$ then leads to Eq. (15).

The limits in Eqs. (14) and (15) are useful to get qualitative insight into the effect of redshift bias and variance when they are small and vary smoothly in redshift. Quantitatively, the finite values of these parameters as well as more general parametrization of these functions may cause the sensitivity of the counts to change from these special limits. In §V, we explore how the sensitivity of the counts to photo-z parameters ultimately affect dark energy constraints.

III. SAMPLE COVARIANCE

The number counts $m_{\alpha,i}(\mathbf{x})$ fluctuate in space tracing the linear density fluctuations $\delta(\mathbf{x})$ induced by large scale structure

$$m_{\alpha,i}(\mathbf{x}) \;=\; \bar{m}_{\alpha,i}[1 + b_\alpha(z)\delta(\mathbf{x})]\,, \quad (19)$$

where $b_\alpha(z)$ is the average cluster linear bias predicted from the distribution in Eq.(4)

$$b_\alpha(z) = \frac{1}{\bar{n}_\alpha(z)}\int\frac{dM}{M}\frac{d\bar{n}_\alpha(z)}{d\ln M}b(M;z)\,, \quad (20)$$

and we take a fit to simulations of [25]

$$b(M;z) = 1 + \frac{a_c\delta_c^2/\sigma^2 - 1}{\delta_c} + \frac{2p_c}{\delta_c[1 + (a\delta_c^2/\sigma^2)^{p_c}]} \quad (21)$$

with $a_c = 0.75$, $p_c = 0.3$, and $\delta_c = 1.69$. From Eq. (19), the counts $m_{\alpha,i}$ then possess a sample covariance given by [26]

$$\begin{aligned} S_{ij}^{\alpha\beta} \;&=\; \langle(m_{\alpha,i} - \bar{m}_{\alpha,i})(m_{\beta,j} - \bar{m}_{\beta,j})\rangle \quad (22)\\ &=\; b_{\alpha,i}\bar{m}_{\alpha,i}b_{\beta,j}\bar{m}_{\beta,j}\int\frac{d^3k}{(2\pi)^3}W_i^*(\mathbf{k})W_j(\mathbf{k})P(k)\,, \end{aligned}$$

which accounts for the clustering of clusters due to large scale structure. Here $W_i(\mathbf{k})$ is the Fourier transform of the window function and for simplicity we assumed that $b_\alpha(z)$ does not vary considerably within the photo-z bin i and can be approximated by $b_\alpha(z) \approx b_\alpha(z_i^p) \equiv b_{\alpha,i}$. In the more general case where $b_\alpha(z)$ varies considerably within the photo-z bin, $W_i(\mathbf{k})$ above would be the Fourier transform of $W_i(\mathbf{x})b_\alpha(z)$, and it would be harder to find an analytical expression for it. We chose not to consider this case since the approximation holds well for the small photo-z bin size ($\delta z^p = 0.1$) considered in our fiducial model.

Let the photo-z bin i be at angular diameter distance $r_i \equiv r(z_i^p)$ and have width $\delta r_i \equiv r(z_{i+1}^{\rm phot}) - r(z_i^{\rm phot})$. Under the assumption that $H(z)$, $z^{\rm bias}(z)$ and $\sigma_z(z)$ also do not change appreciably inside the bin, so that $H(z) \approx H(z_i^p) \equiv H_i$ and likewise for $z^{\rm bias}(z_i^p) \equiv z_i^{\rm bias}$ and $\sigma_z(z_i^p) \equiv \sigma_{z,i}$, the window $W_i(\mathbf{k})$ is given by (see Appendix A)

$$\begin{aligned} W_i(\mathbf{k}) = \quad & 2\exp\left[ik_\parallel\left(r_i + \frac{z_i^{\rm bias}}{H_i}\right)\right]\exp\left[-\frac{\sigma_{z,i}^2k_\parallel^2}{2H_i^2}\right]\\ & \frac{\sin(k_\parallel\delta r_i/2)}{k_\parallel\delta r_i/2}\frac{J_1(k_\perp r_i\theta_s)}{k_\perp r_i\theta_s}\,. \end{aligned} \quad (23)$$

Since $z_i^{\rm bias} \ll \delta z_i^p$ in all practical cases, $b_{\alpha,i}$ and $P(k)$ do not carry any strong dependence on the photo-z bias. In this case, Eqs. (22) and (23) indicate that the sample variance S_{ii} does not depend on $z_i^{\rm bias}$ and is exponentially sensitive to $\sigma_{z,i}^2$. This will bring interesting effects when using sample covariance as a signal for self-calibration (see §V). From Eq. (23), we see that in the

absence of photo-z errors, the window function would suppress modes along the line of sight with wavelengths $\lambda_\parallel < \delta r = \delta z^p/H$. The presence of photo-z scatter further suppresses modes $\lambda_\parallel < \pi\sigma_z/H$. For our fiducial redshift binning of $\delta z^p = 0.1$ we expect significant effects to appear then if $\sigma_z > \delta z^p/\pi \sim 0.03$. As we will see in §V, this is roughly the value of scatter uncertainty where dark energy degradations start to increase considerably.

IV. FISHER MATRIX AND SELF-CALIBRATION

Given a parametrized model that predicts the number counts and their sample covariance, along with a fiducial choice for the true values of these parameters, the Fisher matrix formalism allows us to study the impact of redshift uncertainties on dark energy constraints.

As discussed below, we will consider counts not only in photo-z bins, but also in angular cells and observed mass bins. To simplify the notation, from now on i will index a generalized pixel of redshift, angle and mass whenever these are appropriate and S_{ij} will be the corresponding sample covariance. The total covariance is the sample covariance plus shot variance

$$C_{ij} = S_{ij} + \bar{m}_i \delta_{ij} \, . \tag{24}$$

For convenience, we arrange the counts per pixel i into a vector $\mathbf{m} \equiv (m_1, \ldots, m_{N_{\rm pix}})$ and correspondingly their sample and total covariances into matrices $\mathbf{S}$ and $\mathbf{C}$. The Fisher matrix quantifies the information in the counts on a set of parameters p_α as [6, 27, 28]

$$F_{\alpha\beta} \;=\; \bar{\mathbf{m}}^t_{,\alpha} \mathbf{C}^{-1} \bar{\mathbf{m}}_{,\beta} + \frac{1}{2} {\rm Tr}[\mathbf{C}^{-1}\mathbf{S}_{,\alpha}\mathbf{C}^{-1}\mathbf{S}_{,\beta}] \, . \tag{25}$$

The first term represents the information from the mean counts and the second term carries the information from the sample covariance of the counts. When using only counts information, we will be using only the first term in the Fisher matrix definition, while when using the sample covariance to employ self-calibration we will use both terms. The Fisher matrix approximates the covariance matrix of the parameters $C_{\alpha\beta} \approx [\mathbf{F}^{-1}]_{\alpha\beta}$ such that the marginalized error on a single parameter is $\sigma(p_\alpha) = [\mathbf{F}^{-1}]^{1/2}_{\alpha\alpha}$. When considering prior information on parameters of a given $\sigma(p_\alpha)$ we add to the Fisher matrix a contribution of $\sigma^{-2}(p_\alpha)\delta_{\alpha\beta}$ before inversion.

Next we define our fiducial choices for survey properties and values for cosmological parameters as well as nuisance parameters describing the observable-mass relation and photo-z's.

A. Fiducial Model

We will take a fiducial cluster survey with specifications similar to the South Pole Telescope (SPT) Survey [29]: an area of 4000 deg^2 and a sensitivity corresponding to a constant mass threshold $M^{\rm obs}_{\rm th} = 10^{14.2} h^{-1} M_\odot$. We divide the number counts into photo-z bins of $\delta z^p_i = 0.1$ out to $z^{\rm phot}_{\rm max} = 2$. When using self-calibration from sample variance information, we further divide these counts into 400 angular cells of 10 deg^2. Finally, when employing self-calibration from shape of the observed mass function, we additionally divide the counts in 5 bins of $\Delta \log_{10} M^{\rm obs} = 0.2$. In §V D we will consider some variations on these fiducial choices.

The observable-mass relation will be parametrized by the mass bias $M^{\rm bias}$ and variance $\sigma^2_{\ln M}$ as a function of redshift. Because the evolution in cluster parameters is expected to be smooth in redshift, we will assume in our fiducial model that the mass bias has a power law evolution given by

$$\ln M^{\rm bias}(z) = A_b + n_b \ln(1+z) \tag{26}$$

with fiducial values $A_b = n_b = 0$. For the mass variance $\sigma^2_{\ln M}$ we assume a Taylor expansion around $z = 0$

$$\sigma^2_{\ln M}(z) = \sigma^2_{\ln M}|_{\rm fid} + \sum_{a=0}^{N_\sigma - 1} B_a z^a \tag{27}$$

with fiducial values $\sigma^2_{\ln M}|_{\rm fid} = (0.25)^2$ and $B_a = 0$. We have checked that using a different fiducial value of $\sigma^2_{\ln M}|_{\rm fid} = (0.05)^2$ does not change the results. For the fiducial model we will take a cubic ($N_\sigma = 4$) evolution of the mass variance, so our fiducial model will be comprised of 6 nuisance parameters for the observable-mass distribution. In §V D we also consider a more general parametrization with one value of $M^{\rm bias}$ and $\sigma^2_{\ln M}$ in each photo-z bin.

For the photo-z model we will take the values of $z^{\rm bias}(z)$ and $\sigma^2_z(z)$ in N_z different redshifts as our nuisance photo-z parameters. Values of photo-z parameters at arbitrary values of z are then obtained by cubic spline interpolation. Current photo-z methods can reach accuracies of $\sigma_z \sim 0.1$ for field galaxies up to moderate redshifts ($z \sim 1.4$) when using optical filter band-passes [10] (see also [11] for a case with lower redshifts). If complemented by near-infrared filters, the accuracy can be improved and well controlled up to high redshifts ($z \sim 2.0$). Photo-z's of red early-type galaxies are typically even better because of their very prominent 4000Å break. Finally, cluster photo-z's are expected to be further improved by averaging the photo-z's of individual cluster galaxies. However, this will only be the case if the presence of interlopers is small and well understood. We expect therefore not only the photo-z errors to be smaller than the corresponding errors for field galaxies, but the error distribution to be more well behaved. For instance the Gaussian assumption of Eq. (6) should be a good approximation for clusters with well understood selections. For our fiducial photo-z model, we will take $N_z = 20$, i.e. one value of $z^{\rm bias}$ and σ^2_z for each bin $\delta z = 0.1$ of *true* redshift. We will assume fiducial values $z^{\rm bias}(z)|_{\rm fid} = 0$

and

$$\sigma_z(z)|_{\rm fid} = 0.03(1+z) \tag{28}$$

to account for the fact that the photo-z scatter is expected to increase at high redshifts. In §V D , we consider a different photo-z model with a constant $\sigma_z(z)|_{\rm fid} = 0.02$, and show that the results are very similar to the ones in the fiducial model. That the results are insensitive to the fiducial values assumed in a given parametrization is a check of the validity of our Fisher matrix approach. Obviously, changes in the parametrization and in the number of nuisance parameters affect the results. The choice of $N_z = 20$, corresponding to one value of $z^{\rm bias}$ and σ_z^2 per photo-z bin used to count clusters (recall $\delta z_i^p = 0.1$) is, although natural, arbitrary. In principle, we could choose $N_z = 10$ or 40 and keep the same photo-z binning or alternatively use coarser/finer photo-z bins. The photo-z bin size is ultimately dictated by the photo-z precision that can be achieved, e.g. the photo-z bin size should be larger than $z^{\rm bias}$ or σ_z. The value of $\delta z_i^p = 0.1$ chosen reflects conservative expectations for the photo-z precision of future cluster surveys. In §V D we consider alternative models with $N_z = 10$ and $\delta z_i^p = 0.2$.

For the fiducial cosmological parameters, we will assume a flat universe and take parameter values based on the results of the Wilkinson Microwave Anisotropy Probe first year data release (WMAP1). In §V D we will also consider a fiducial cosmology based on the third year data release (WMAP3). We chose the WMAP1 as the fiducial case since this cosmology will place the stronger requirements on the photo-z errors. For the WMAP1 case, the cosmological parameters are the normalization of the initial curvature spectrum $\delta_\zeta (= 5.07 \times 10^{-5})$ at $k = 0.05$ Mpc^{-1} (corresponding to $\sigma_8 = 0.91$, see [30]), its tilt $n(= 1)$, the baryon density $\Omega_b h^2 (= 0.024)$, the dark matter density $\Omega_m h^2 (= 0.14)$, and the two dark energy parameters of interest: its density $\Omega_{\rm DE} (= 0.73)$ relative to critical and equation of state $w(= -1)$ which we assume to be constant. The fiducial values are given in parentheses. For the WMAP3 cosmology we take $\delta_\zeta (= 4.53 \times 10^{-5})$ at $k = 0.05$ Mpc^{-1} (corresponding to $\sigma_8 = 0.76$), $n(= 0.958)$, $\Omega_b h^2 (= 0.0223)$, $\Omega_m h^2 (= 0.128)$, $\Omega_{\rm DE} (= 0.76)$ and $w(= -1)$. We will assume 1% priors on all cosmological parameters except for the dark energy parameters, which will vary freely.

V. RESULTS

Now we apply the formalism developed in §IV to study how dark energy constraints are affected by redshift uncertainties. We first consider the case where masses are perfectly known and only information from counts is used to constrain dark energy. We then progress to a more pessimistic case where masses are unknown and self-calibration is employed in a joint fit of dark energy and observable-mass parameters. We then consider the case where masses are known, and self-calibration is used to reduce the redshift requirements. Finally, we study how stable our results are to changes in our fiducial parametrization and estimate the requirements on the size of calibration training sets necessary in order not to degrade dark energy constraints appreciably.

Given the values of the prior uncertainties in the redshift bias $\sigma(z^{\rm bias})$ and variance $\sigma(\sigma_z^2)$, which produce the constraint $\sigma(w) = \sigma\left[w|\sigma(z^{\rm bias}), \sigma(\sigma_z^2)\right]$ on the dark energy equation of state w, we define the w degradation d_w relative to a reference case with w constraint $\sigma(w)|_{\rm ref} < \sigma(w)$ as

$$d_w(\sigma(z^{\rm bias}), \sigma(\sigma_z^2)) = \frac{\sigma\left[w|\sigma(z^{\rm bias}), \sigma(\sigma_z^2)\right]}{\sigma(w)|_{\rm ref}} - 1 \tag{29}$$

and likewise for the $\Omega_{\rm DE}$ degradation $d_{\Omega_{\rm DE}}$. Unless otherwise specified, we will take the reference case to be the baseline case of perfect redshifts $\sigma(w)|_{\rm ref} = \sigma\left[w|0,0\right]$. In some cases though we will also use this degradation definition to generally compare two different scenarios such as the WMAP1 versus WMAP3 cosmologies and implementations assuming masses to be perfectly known versus self-calibrated.

A. Perfect Mass Calibration

In the case of perfect knowledge of the observable-mass relation, the dark energy constraints from cluster counts alone are quite strong, as long as we have a reasonable knowledge of redshifts parameters. In the case of perfect redshifts, the baseline constraints are $\sigma(w, \Omega_{\rm DE}) = (0.033, 0.0081)$ in the fiducial model.

These constraints are degraded as the uncertainties in the redshift bias and variance increase. With counts information only, interesting dark energy constraints can only be extracted if we have some prior knowledge of both redshift bias and scatter uncertainties, i.e. no constraints can be extracted if either $\sigma(z^{\rm bias}) \to \infty$ or $\sigma(\sigma_z^2) \to \infty$.

The top panels of Fig. 2 show the degradations in dark energy for finite values of redshift uncertainties. The top left panel shows d_w and $d_{\Omega_{\rm DE}}$ as a function of $\sigma(z^{\rm bias})$ (with $\sigma(\sigma_z^2) = 0$) and as a function of $\sigma(\sigma_z^2)$ (with $\sigma(z^{\rm bias}) = 0$). The top right panel shows contours of fixed d_w values in the plane defined by values of $\sigma(z^{\rm bias})$ and $\sqrt{\sigma(\sigma_z^2)}$. Table I shows constraints and degradations in the fiducial model for the case of perfect masses and for the self-calibration cases of §V B and §V C. As expected, the dark energy constraints are more sensitive to the photo-z bias compared to the photo-z scatter by about an order of magnitude.

B. Mass Self-Calibration

Now we consider the case where we do not know the observable-mass parameters and solve for them along with dark energy parameters simultaneously by means of self-calibration with clustering and shape information.

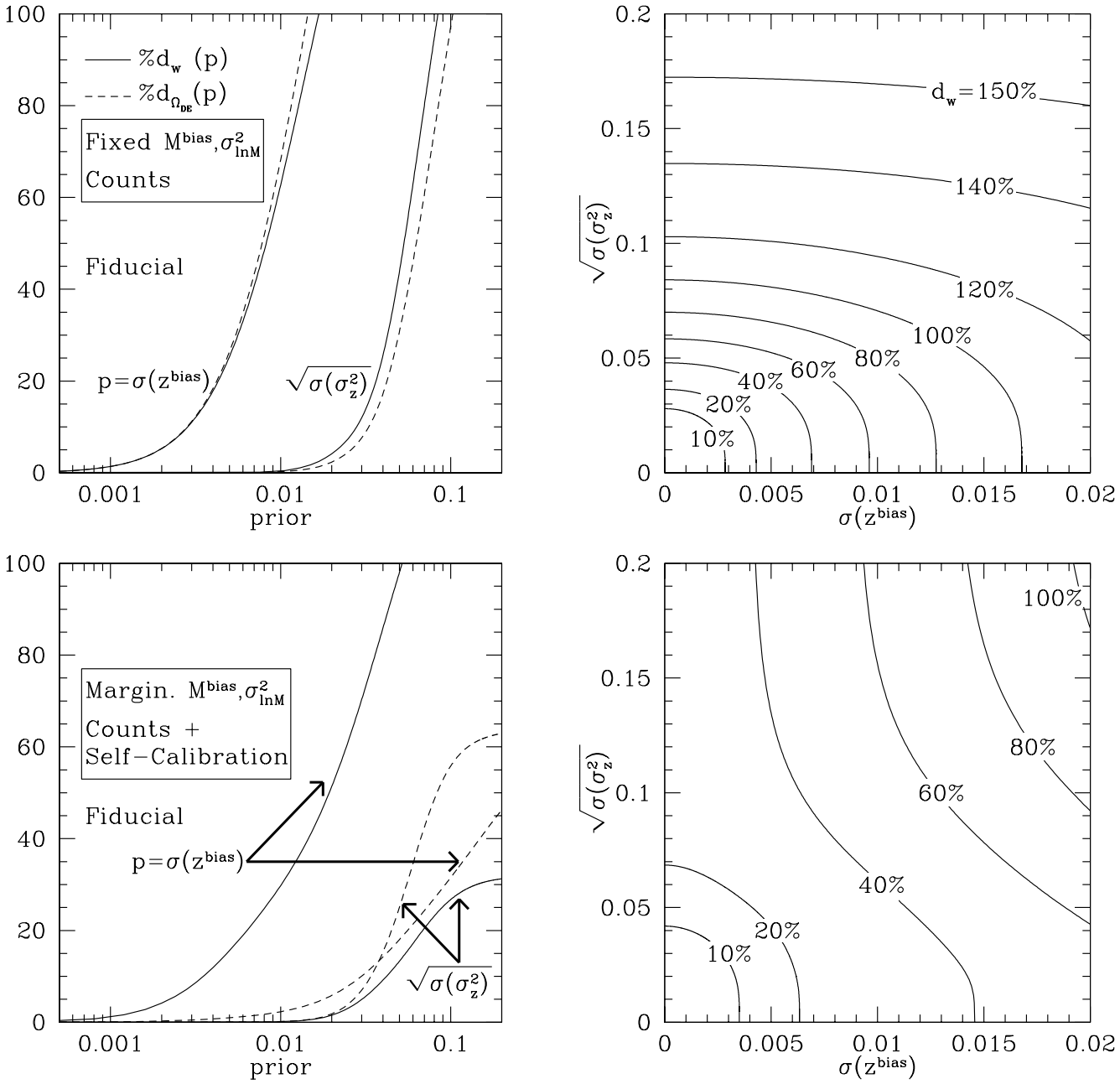

FIG. 2: Dark energy sensitivity to prior knowledge of redshift parameters in the WMAP1 cosmology and fiducial model described in §IV. The *top row* displays results for the case of perfect masses employing only counts information. The *bottom row* is for the case of marginalized observable-mass parameters and self-calibration with clustering and shape information. The *left panels* show percent degradation in dark energy parameter constraints with respect to case of perfect redshift knowledge as a function of prior uncertainty in $z^{\rm bias}$ for fixed σ_z^2 and as a function of prior uncertainty in σ_z^2 for fixed $z^{\rm bias}$. The *right panels* display the respective contours of fixed degradation d_w in the $\sigma(z^{\rm bias})$ versus $\sqrt{\sigma(\sigma_z^2)}$ plane. Compared to perfect masses, in the case of self-calibration dark energy degradations are weaker due to (i) worse baseline constraints and (ii) decreased degeneracies between dark energy and photo-z parameters, partially broken by self-calibration.

Let us consider first the case of perfect redshifts. Self-calibration results are shown in Fig. 3 for our fiducial model. For reference, the case of perfect masses is displayed in the black solid ellipsis corresponding to the tight baseline constraints of §V A. If no self-calibration of the observable-mass relation is used in a joint fit of mass and dark energy parameters, no interesting constraints can be extracted. Keeping redshifts fixed, assuming the functional forms of Eqs. (26), (27) for the mass bias and variance and employing self-calibration from clustering information in the sample covariance of counts produces constraints $\sigma(w, \Omega_{\rm DE}) = (0.23, 0.22)$. Further

Observable-Mass parameters		Information	Constraints		Degradations	
$\ln M^{\rm bias}$	$\sigma^2_{\ln M}$		$\sigma(w)$	$\sigma(\Omega_{\rm DE})$	d_w	$d_{\Omega_{\rm DE}}$
Known	Known	Counts	0.033	0.0081	21%	17%
Known	Marginalized	Counts	0.19	0.21	90%	108%
Marginalized	Marginalized	Counts	-	-	-	-
Known	Known	Counts + Self-Calibration	0.031	0.0078	16%	15%
Known	Marginalized	Counts + Self-Calibration	0.072	0.019	5%	3%
Marginalized	Marginalized	Counts + Self-Calibration	0.12	0.029	11%	8.3%

TABLE I: Dark energy baseline constraints and degradations for the fiducial model with observable-mass parameters known/marginalized and with/without self-calibration. Baseline constraints $\sigma(w)$ and $\sigma(\Omega_{\rm DE})$ are for $\sigma(z^{\rm bias}) = \sigma(\sigma_z^2) = 0$ and degradations d_w and $d_{\Omega_{\rm DE}}$ relative to the baseline are for $\sigma(z^{\rm bias}) = 0.003$ and $\sqrt{\sigma(\sigma_z^2)} = 0.03$.

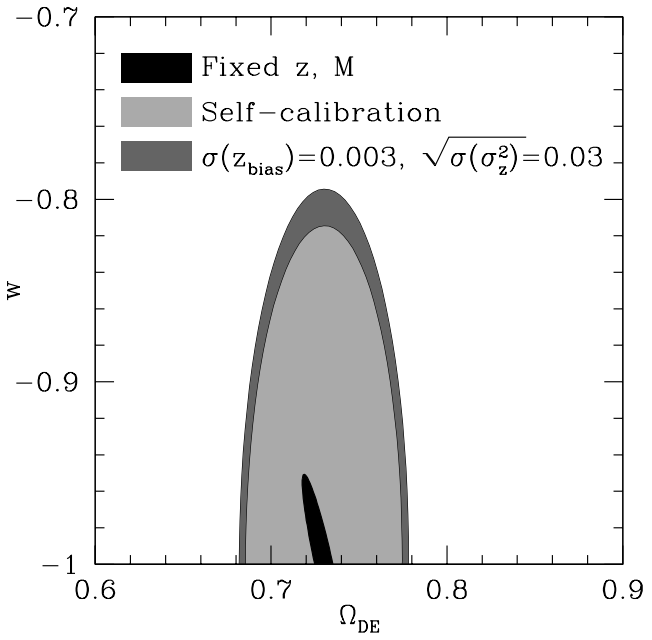

FIG. 3: Dark energy constraints for the fiducial model in the WMAP1 cosmology. From inner to outer ellipses, the 68% CL regions are shown for the case where redshift and mass parameters are perfectly known (black); the case with self-calibration from sample covariance and shape information but fixed photo-z parameters (light gray); the case with self-calibration and prior uncertainties on photo-z parameters of $\sigma(z^{\rm bias}) = 0.003$ and $\sqrt{\sigma(\sigma_z^2)} = 0.03$ (dark gray). The latter case corresponds to a degradation of $d(w, \Omega_{\rm DE}) = (11\%, 8.3\%)$ with respect to the case of fixed redshifts.

adding shape information from multiple mass bins allows a good degree of self-calibration as shown in the light gray ellipsis of Fig. 3; the constraints in this case are $\sigma(w, \Omega_{\rm DE}) = (0.12, 0.029)$, i.e. there is a degradation of $d(w, \Omega_{\rm DE}) = (280\%, 260\%)$ with respect to the case of perfect mass in §V A.

As the uncertainty in redshift parameters increases, the ability to self-calibrate masses is reduced. The dark gray ellipsis in Fig. 3 shows how the self-calibrated case above is degraded if we take the photo-z parameters to have uncertainties of $\sigma(z^{\rm bias}) = 0.003$ and $\sqrt{\sigma(\sigma_z^2)} = 0.03$ simultaneously as opposed to being fixed; in this case the constraints are $\sigma(w, \Omega_{\rm DE}) = (0.14, 0.032)$, i.e. a degradation of $d(w, \Omega_{\rm DE}) = (11\%, 8.3\%)$. The dark energy degradation in the case of self-calibration is shown in the bottom panels of Fig. 2 and in the bottom rows of Table I. Notice that because the baseline constraints (perfect redshifts) are worse with self-calibration compared to fixed masses, the degradation relative to the baseline is correspondingly weaker. The weaker degradation is partially because the baseline constraints are worse, but also because self-calibration helps break not only the degeneracy between dark energy and mass, but also redshifts. In §V C we investigate that further.

C. Redshift Self-Calibration

If external mass calibrations can partially or totally constrain the mass bias or scatter or both, self-calibration is still useful to monitor redshifts, therefore decreasing the redshift requirements. More generally, self-calibration provides important consistency checks that theoretical assumptions and observations agree, even more so when we have stringent external mass priors. External mass calibrations can come for instance from follow-up of a small sample of clusters with very well measured masses, weak lensing calibrations, simulations, etc.

Let us consider the limiting case where external calibrations put strong priors on the mass bias, but no prior on the mass scatter, i.e. $\sigma(\ln M^{\rm bias}) = 0$ and $\sigma(\sigma^2_{\ln M}) = \infty$. In this case, without self-calibration, the constraints for perfect redshifts are $\sigma(w, \Omega_{\rm DE}) = (0.19, 0.21)$ and they degrade to $\sigma(w, \Omega_{\rm DE}) = (0.35, 0.44)$, i.e. a degradation of $d(w, \Omega_{\rm DE}) = (90\%, 108\%)$ if we impose redshift priors of $\sigma(z^{\rm bias}) = 0.003$ and $\sqrt{\sigma(\sigma_z^2)} = 0.03$. Employing self-calibration the constraints for perfect redshifts $\sigma(w, \Omega_{\rm DE}) = (0.072, 0.019)$ degrade to $\sigma(w, \Omega_{\rm DE}) = (0.076, 0.019)$ with the same redshift priors, i.e. a degradation of only $d(w, \Omega_{\rm DE}) = (5\%, 3\%)$.

Consider now the limiting case where external priors can further constrain the mass scatter to $\sigma(\sigma^2_{\ln M}) = 0$ in addition to the mass bias. Without self-calibration, the constraints for perfect redshifts are $\sigma(w, \Omega_{\rm DE}) = (0.033, 0.0081)$ and they degrade to $\sigma(w, \Omega_{\rm DE}) = (0.039, 0.095)$ if we impose redshift priors of $\sigma(z^{\rm bias}) = 0.003$ and $\sqrt{\sigma(\sigma_z^2)} = 0.03$. , i.e. a degradation of $d(w, \Omega_{\rm DE}) = (21\%, 17\%)$. Employing self-calibration the constraints for perfect redshifts $\sigma(w, \Omega_{\rm DE}) = (0.031, 0.0078)$ degrade to $\sigma(w, \Omega_{\rm DE}) = (0.036, 0.0090)$ with the same redshift priors, i.e. a degradation of $d(w, \Omega_{\rm DE}) = (16\%, 15\%)$. These results are also displayed in Table I. Interestingly, in the limit where we have no redshift knowledge ($\sigma(z^{\rm bias}) = \sigma(\sigma_z^2) = \infty$), without self-calibration no interesting dark energy constraints are possible, but employing full self-calibration we can still obtain $\sigma(w, \Omega_{\rm DE}) = (0.11, 0.11)$.

These results show that self-calibration is very effective not only in allowing a joint fit of mass and cosmological parameters, but also in reducing the redshift requirements in those cases. As external priors put constraints on some of the observable-mass relation parameters, but not all of them, self-calibration becomes even more important. In the limit where external priors are even stronger and masses are perfectly determined, self-calibration becomes less important, but it still helps monitor redshifts. However, even in this case prior redshift knowledge is still important in order to extract the survey full constraining power. Since any given survey is likely to be in between these limit cases, both self-calibration techniques and good knowledge of redshifts will be comparably important.

D. Fiducial Model Dependence

In this section we consider deviations from our fiducial model and their effect on the dark energy degradation results. Even though changes in the fiducial values of the nuisance parameters describing the observable-mass relation and photo-z's have a very small effect on the constraints, changes in their parametrization will obviously affect the results. For instance, increasing the number of parameters in the mass-observable relation to allow for more general models produces worse baseline constraints and correspondingly weaker degradations due to photo-z uncertainties. The constraints obviously also change if the fiducial cosmology and survey specifications deviate considerably from the ones assumed in the fiducial model. We will first consider a fiducial cosmology based on cosmological parameters from WMAP3 and also changes in our fiducial survey properties. Finally we will consider deviations in the photo-z model assumed.

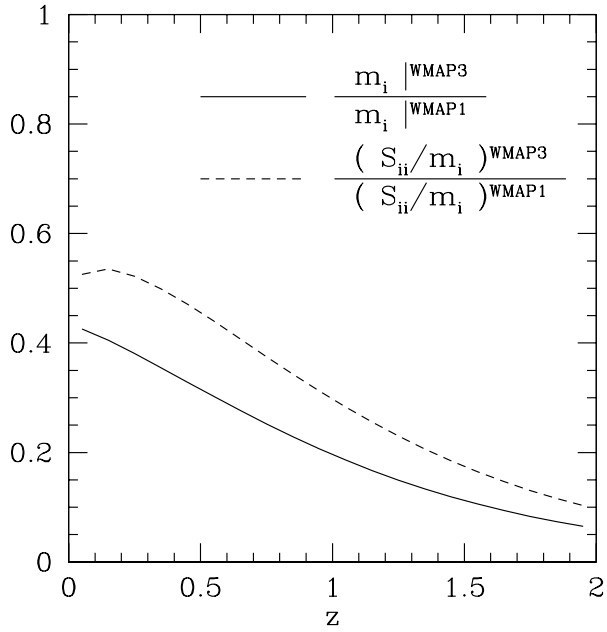

FIG. 4: The lower value of σ_8 in the WMAP3 cosmology decreases the number counts with respect to WMAP1, specially at high redshift. Similarly, the relative importance of sample variance errors with respect to the increased shot noise decreases, lowering the power of using sample variance as a signal for self-calibration.

1. *Fiducial Cosmology and Survey Properties*

Because of the exponential sensitivity of the cluster mass function to the growth of structure, the decrease in the value of σ_8 for WMAP3 causes the overall number counts to be reduced by a factor of ~ 4 with respect to the WMAP1 case. Likewise, the reduction in counts decreases the relative importance of sample variance errors with respect to Poisson shot noise. In Fig. 4 we show the ratio of the average number counts $m_i(z)$ in the WMAP3 and WMAP1 cosmologies, as well as the ratio of the corresponding sample variance S_{ii} relative to Poisson variance m_i.

Let us first consider the case of perfect knowledge of the observable-mass parameters. In the case of perfect redshifts, the baseline constraints for the WMAP3 cosmology with count information become $\sigma(w, \Omega_{\rm DE}) = (0.047, 0.010)$. Even though the WMAP3 total number counts are reduced by a factor of ~ 4 compared to WMAP1, the baseline constraints degrade only by $d(w, \Omega_{\rm DE}) = (44\%, 25\%)$. If all clusters carried the same cosmological information, we would naively expect a factor of ~ 2 degradation from the increased Poisson errors. However, the rare high mass/redshift clusters are more sensitive to cosmology. The fact that the relative reduction on the number of these rare clusters is more pronounced provides extra cosmology information that partially balances the degradation from the overall counts reduction.

Case	Number Counts per deg^2	Observable-Mass parameters	Information	Constraints		Degradations	
				$\sigma(w)$	$\sigma(\Omega_{\rm DE})$	d_w	$d_{\Omega_{\rm DE}}$
Fiducial model	8.0	Known	Counts	0.033	0.0081	21%	17%
WMAP3	2.1	Known	Counts	0.047	0.010	5.7%	6.1%
$M_{\rm th}^{\rm obs} = 10^{14.435} h^{-1} M_\odot$	2.1	Known	Counts	0.050	0.012	5.6%	5.8%
Area = 1000 deg^2	2.0	Known	Counts	0.054	0.014	4.9%	3.5%
$z_{\rm max}^{\rm phot} = 0.5$	2.3	Known	Counts	0.063	0.015	410%	780%
Fiducial model	8.0	Marginalized	Counts + Self-Calibration	0.12	0.029	11%	8.3%
WMAP3	2.1	Marginalized	Counts + Self-Calibration	0.24	0.048	7.0%	6.2%
$M_{\rm th}^{\rm obs} = 10^{14.435} h^{-1} M_\odot$	2.1	Marginalized	Counts + Self-Calibration	0.24	0.052	7.3%	5.4%
Area = 1000 deg^2	2.0	Marginalized	Counts + Self-Calibration	0.24	0.052	4.0%	2.9%
$z_{\rm max}^{\rm phot} = 0.5$	2.3	Marginalized	Counts + Self-Calibration	0.28	0.034	35%	42%

TABLE II: Dark energy baseline constraints and degradations for the fiducial model (WMAP1, $M_{\rm th}^{\rm obs} = 10^{14.2} h^{-1} M_\odot$, Area = 4000 deg^2, $z_{\rm max}^{\rm phot} = 2.0$) and various deviations from the fiducial survey properties and cosmology. In all cases the total number of clusters is reduced by a factor of ~ 4 with respect to the fiducial case. Baseline constraints are for $\sigma(z^{\rm bias}) = \sigma(\sigma_z^2) = 0$ and relative degradations are for $\sigma(z^{\rm bias}) = 0.003$ and $\sqrt{\sigma(\sigma_z^2)} = 0.03$.

Let us now consider the dark energy degradations due to photo-z uncertainties. The top panel of Fig. 5 shows the degradation of dark energy parameters as a function of photo-z uncertainties for the WMAP3 cosmology. Notice that dark energy degradations relative to the baseline cases are slightly weaker for the WMAP3 case, since its baseline is worse, confirming the trend that surveys with smaller yields require less knowledge of redshift parameters for fixed baseline degradations. In other words, in the limit of perfect masses for the WMAP3 case, dark energy constraints are less sensitive to photo-z uncertainties because the best achievable results are worse.

Now we consider the case where we marginalize over the observable-mass parameters and employ self-calibration. In this case, with perfect redshifts the constraints for WMAP3 are $\sigma(w, \Omega_{\rm DE}) = (0.24, 0.048)$, i.e. a degradation of $d(w, \Omega_{\rm DE}) = (410\%, 370\%)$ with respect to the case of perfect masses and $d(w, \Omega_{\rm DE}) = (96\%, 64\%)$ with respect to the corresponding self-calibrated case in the WMAP1 cosmology. Self-calibration is based on the ability to divide the cluster sample in space and mass. The decrease in the number counts for WMAP3 reduces the relative importance of sample variance over the increased shot noise, and reduces the power of self-calibration by clustering. In addition, the ability to split the sample in mass bins is decreased because we run out of clusters at high masses, and self-calibration from shape information is also reduced.

The bottom panel of Fig. 5 shows the dark energy degradation as a function of photo-z uncertainties for the case of self-calibration in the WMAP3 cosmology. Relative to the case of perfect masses and to the self-calibrated case of WMAP1, most degradations for WMAP3 are weaker, as expected from the worse baseline constraints. However the $\sigma(\Omega_{\rm DE})$ degradation as a function $\sqrt{\sigma(\sigma_z^2)}$ is stronger relative to both cases. That happens because self-calibration uses sample covariance information, which is exponentially sensitive to σ_z^2. With the reduced relative importance of sample variance in WMAP3, changes in σ_z^2 are now relatively more degenerate with cosmology and observable-mass parameters.

To make the point clearer, let us consider the case where we employ self-calibration only from shape information, but not clustering. In this case the self-calibration constraints for perfect redshifts are $\sigma(w, \Omega_{\rm DE}) = (0.26, 0.11)$, i.e. the w constraint is nearly identical to the full self-calibration case, but the $\Omega_{\rm DE}$ constraint is still ~ 2 times higher. Keeping the photo-z bias fixed $\sigma(z^{\rm bias}) = 0$ and applying a prior on the photo-z variance of $\sqrt{\sigma(\sigma_z^2)} = 0.2$, the constraints degrade to $\sigma(w, \Omega_{\rm DE}) = (0.87, 0.17)$, i.e. a degradation of $d(w, \Omega_{\rm DE}) = (240\%, 54\%)$. With full self-calibration the corresponding degradation is $(30\%, 110\%)$. Therefore whereas clustering self-calibration from sample variance does not help the w constraint to further decrease considerably from its value with shape self-calibration only, it does make this constraint less sensitive to photo-z uncertainties. On the other hand, clustering self-calibration improves the $\Omega_{\rm DE}$ constraint, but leaves it more unstable to photo-z scatter uncertainties. These features tell us that, when employing self-calibration, knowledge of the photo-z scatter is essential, specially in a situation of fewer clusters such as in the WMAP3 cosmology.

For completeness, we consider other survey modifications that lead to roughly the same reduction in the total number counts as the WMAP3 cosmology relative to WMAP1. Table II shows results for the fiducial model along with the WMAP3 case and changes in the mass threshold $M_{\rm th}^{\rm obs}$, total survey area, and maximum survey redshift $z_{\rm max}^{\rm phot}$. All cases lead to a reduction in the total counts by a factor of ~ 4 relative to the fiducial model. In the case where we change the maximum redshift to $z_{\rm max}^{\rm phot} = 0.5$, we also reduce the number of photo-z parameters to $N_z = 5$ so as to keep one value of $z^{\rm bias}$ and

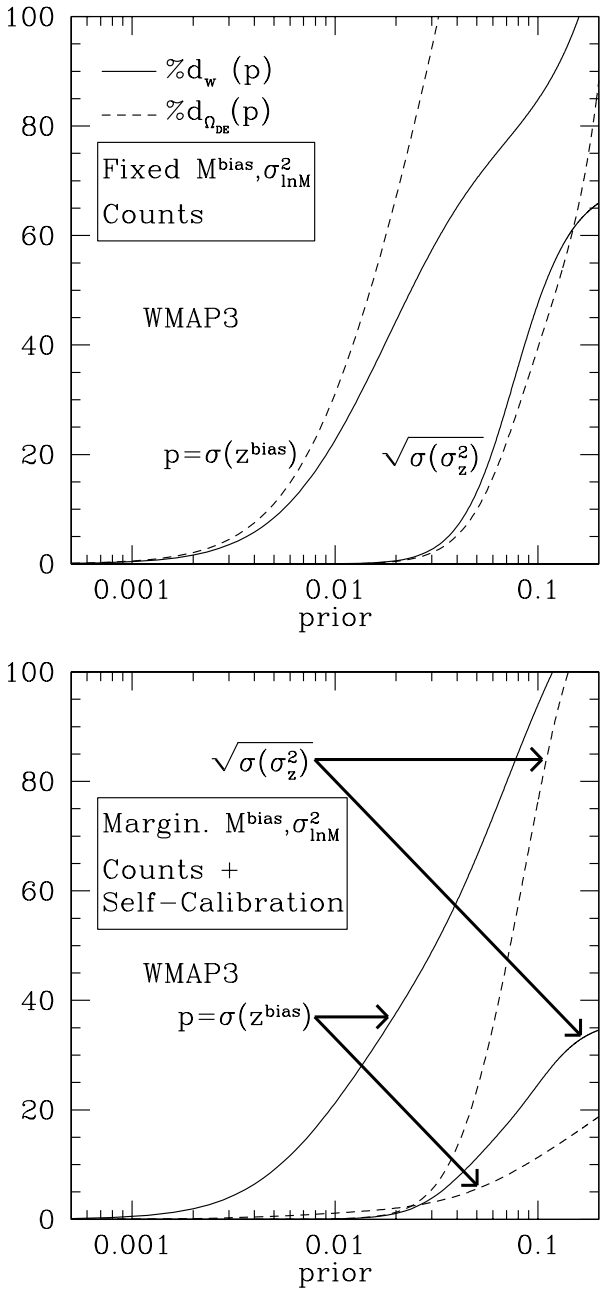

FIG. 5: Degradation in dark energy parameters similar to Fig. 2 but for the WMAP3 cosmology.

σ_z^2 per photo-z bin of $\delta z_i^p = 0.1$. Except for the change in $z_{\rm max}^{\rm phot}$, which makes dark energy constraints and degradations much worse, all other cases produce results roughly similar. Obviously, although these changes produce similar counts reduction, they all remove different clusters. For instance, the WMAP3 reduction is more pronounced at high redshifts, whereas the change in $M_{\rm th}^{\rm obs}$ removes all low mass clusters and the change in survey area reduces the numbers of all clusters equally.

In the case of perfect masses and counts only, except for the $z_{\rm max}$ reduction case, the cases with worse baseline constraints have weaker degradations; the more drastic change of reducing $z_{\rm max}^{\rm phot}$ has a much higher impact because with the total removal of high redshift clusters, the leverage to probe the evolution of the growth of structure is severely diminished.

In the case of self-calibration, many factors affect the degradations. For the fiducial model and the cases of decrease in area and $z_{\rm max}^{\rm phot}$, the degradations are smaller compared to the case of only counts, because their baseline constraints are much worse and self-calibration is fairly efficient. Even though the degradation in the case of $z_{\rm max}^{\rm phot}$ reduction is still the highest, it is many times smaller than in the case of counts only, because with this small redshift range, self-calibration is able to break most of the high degeneracy between mass, redshift and cosmology. For the cases of WMAP3 and reduction in $M_{\rm th}^{\rm obs}$, the degradations are larger compared to counts only and perfect masses. In the WMAP3 case self-calibration is harder because of the reduction in σ_8, which lowers the value of S_{ii}. In the case of reduction in $M_{\rm th}^{\rm obs}$, the removal of the low mass clusters makes self-calibration from shape information harder. In any case, we confirm the trend that more ambitious surveys will be able to extract more information from self-calibration techniques but will also require more redshift knowledge for a full realization of their constraining power.

2. Fiducial Observable-Mass Parameters

Now we return to the WMAP1 cosmology case, but we change our fiducial parametrization of the observable-mass relation. We allow the mass bias and variance to be general functions of redshift, i.e. instead of assuming the functional forms in Eqs. (26) and (27), we now have one value of $M^{\rm bias}$ and $\sigma^2_{\ln M}$ in each photo-z bin of $\delta z_i^p = 0.1$. For the case of fixed mass parameters, the dark energy constraints obviously do not change, but they become $\sigma(w, \Omega_{\rm DE}) = (0.22, 0.030)$, i.e. a degradation of $d(w, \Omega_{\rm DE}) = (80\%, 4\%)$ with respect to the fiducial model with self-calibration.

In Fig. 6 we show the corresponding dark energy degradation from the baseline constraints as a function of photo-z uncertainties in this case. Now $\sigma(w)$ has a worse baseline, and its degradation is less sensitive to $\sigma(z^{\rm bias})$ but more sensitive to $\sigma(\sigma_z^2)$ compared to the fiducial model. On the other hand, since the baseline $\sigma(\Omega_{\rm DE})$ basically did not change, meaning that it is making strong use of self-calibration, its degradation as a function of $\sigma(z^{\rm bias})$ is nearly identical, but is much stronger as a function of $\sigma(\sigma_z^2)$. In this conservative case of 40 parameters for the observable-mass relation, where self-calibration is being used in its full power, if we are interested in moderate dark energy degradations ($\sim 10\% - 20\%$), both $\sigma(z^{\rm bias})$ and $\sigma(\sigma_z^2)$ are important. As we transit to the case with fewer parameters, $\sigma(z^{\rm bias})$ becomes relatively more important.

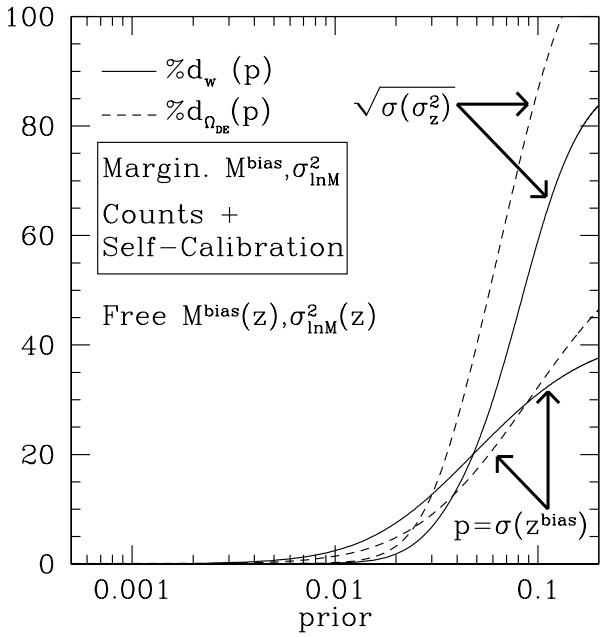

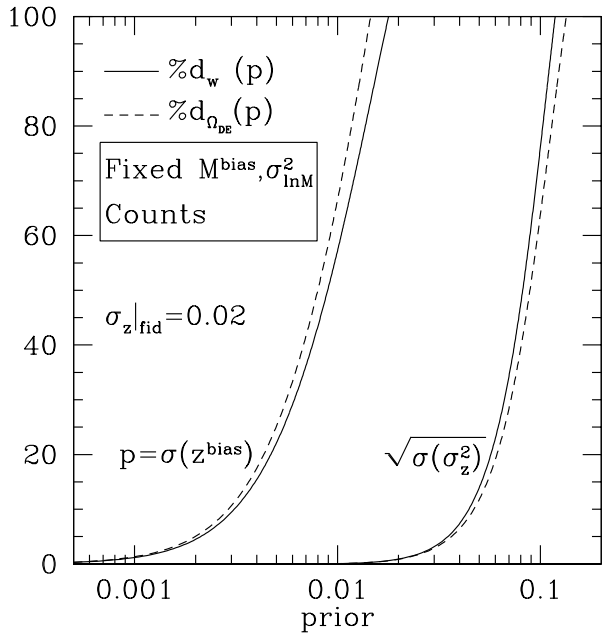

FIG. 6: Degradation in dark energy parameters for the case where $M^{\rm bias}$ and $\sigma^2_{\ln M}$ are free functions of redshift as opposed to having the functional forms of Eqs. (26), (27) assumed in our fiducial model.

3. *Fiducial Photo-z Parameters*

Finally, we consider the case where Eq. (28) in our fiducial model is replaced by a fiducial photo-z scatter of $\sigma_z|_{\rm fid} = 0.02$ constant in redshift. Let us consider the case of perfect masses first. In the case of perfect redshifts the baseline constraints in this case are $\sigma(w, \Omega_{\rm DE}) = (0.032, 0.080)$, i.e. they remain nearly the same as in our fiducial case ($\sim 1\%$ improvement). In the top panel of Fig. 7 we show dark energy degradations as we allow for uncertainties in photo-z parameters. Since the $z^{\rm bias}$ model is still the same, degradations as a function of $\sigma(z^{\rm bias})$ are identical to the fiducial case. As a function of $\sqrt{\sigma(\sigma_z^2)}$ they are only slightly weaker.

In the case of self-calibration, the baseline constraints are $\sigma(w, \Omega_{\rm DE}) = (0.11, 0.026)$, i.e. they improved by $(6\%, 10\%)$ with respect to the corresponding self-calibrated case in the fiducial model. Now the improvement is more noticeable than in the case of perfect masses since we use sample variance to self-calibrate mass parameters. In the bottom panel of Fig. 7 we show dark energy degradations in this case. Again, degradations as functions of $\sigma(z^{\rm bias})$ are identical to the fiducial model. As a function of $\sqrt{\sigma(\sigma_z^2)}$ degradations become stronger at lower values of $\sigma(\sigma_z^2)$, since we are now in a better baseline. At higher values of $\sigma(\sigma_z^2)$, degradations become weaker, since self-calibration is now more efficient.

Finally, let us consider the effect of changing the number of photo-z parameters N_z and/or the photo-z bin size δz^p. In Table III we show the fiducial model and

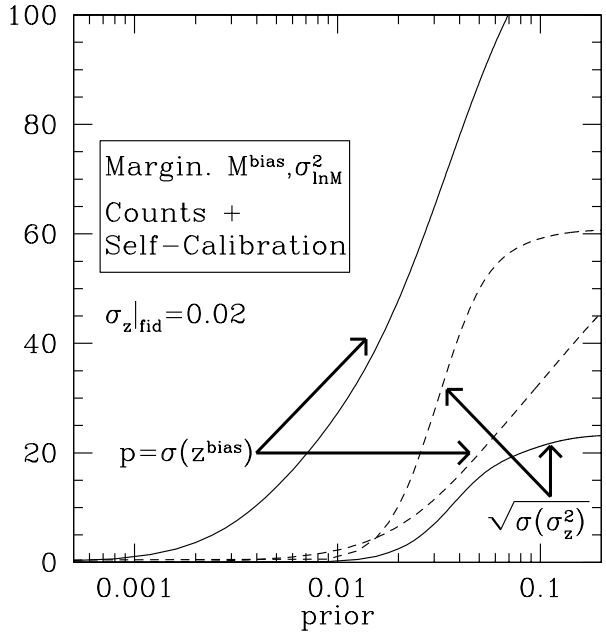

FIG. 7: Dark energy parameters degradation for a fiducial photo-z scatter of $\sigma_z|_{\rm fid} = 0.02$ constant in redshift as opposed to the fiducial model of Eq. (28).

variations in the photo-z model that include changes in the fiducial values of the photo-z scatter, N_z and δz^p. The degradations are shown for priors of $\sigma(z^{\rm bias}) = 0.003\sqrt{N_z/20}$ and $\sigma(\sigma_z^2) = (0.03)^2\sqrt{N_z/20}$. The scaling of the priors with N_z comes from Eqs. (30),(31) and the fact that the number $N_{\rm spec}$ of spectroscopic calibrators in a given redshift region is inversely proportional to the number of redshift bins $N_{\rm spec} \propto 1/N_z$. These scaled priors then reflect constraints per fixed bin $\delta z = 0.1$ of *true* redshift independently of the value of N_z used. No-

Case	Observable-Mass parameters	Information	Constraints		Degradations	
			$\sigma(w)$	$\sigma(\Omega_{\rm DE})$	d_w	$d_{\Omega_{\rm DE}}$
Fiducial model	Known	Counts	0.033	0.0081	21%	17%
$\sigma_z\|_{\rm fid}=0.02$	Known	Counts	0.032	0.0080	12%	13%
$N_z=10$ and $\delta z^p=0.1$	Known	Counts	0.033	0.0081	15%	15%
$N_z=20$ and $\delta z^p=0.2$	Known	Counts	0.033	0.0083	51%	52%
$N_z=10$ and $\delta z^p=0.2$	Known	Counts	0.033	0.0083	14%	14%
Fiducial model	Marginalized	Counts + Self-Calibration	0.12	0.029	11%	8.3%
$\sigma_z\|_{\rm fid}=0.02$	Marginalized	Counts + Self-Calibration	0.11	0.026	15%	30%
$N_z=10$ and $\delta z^p=0.1$	Marginalized	Counts + Self-Calibration	0.12	0.029	13%	14%
$N_z=20$ and $\delta z^p=0.2$	Marginalized	Counts + Self-Calibration	0.13	0.031	22%	6.1%
$N_z=10$ and $\delta z^p=0.2$	Marginalized	Counts + Self-Calibration	0.13	0.031	11%	4.8%

TABLE III: Dark energy baseline constraints and degradations for the fiducial model ($\sigma_z|_{\rm fid}=0.03(1+z)$, $N_z=20$ and $\delta z^p=0.1$) and deviations from the fiducial photo-z parameters. Baseline constraints are for $\sigma(z^{\rm bias})=\sigma(\sigma_z^2)=0$ and relative degradations are for $\sigma(z^{\rm bias})=0.003\sqrt{N_z/20}$ and $\sigma(\sigma_z^2)=(0.03)^2\sqrt{N_z/20}$. The priors are scaled to reflect constraints per fixed bin $\delta z=0.1$ of *true* redshift.

tice from Table III that the baseline constraints do not change much by doing this changes in the fiducial model but the degradations relative to the baseline are affected by a series of competing effects.

Decreasing the number of photo-z parameters to $N_z=10$ while keeping the photo-z bin size at $\delta z_i^p=0.1$ (i) partially decreases some degeneracies between dark energy and the fewer photo-z parameters and (ii) makes the photo-z parameters smoother functions of redshift, making photo-z perturbations more nonlocal (less restricted to a particular photo-z bin). The latter effect causes (a) the counts sensitivity to $z^{\rm bias}$ to increase because it depends on the value of $z^{\rm bias}$ at the bin borders, and (b) the sensitivity to σ_z^2 decreases because the number of objects scattered up, controlled by the values of σ_z at the bin borders, more efficiently compensates the number of objects scattered down, controlled by σ_z at the bin center. In the case of counts only and perfect mass the dark energy degradations are weaker than the fiducial case whereas in the case of unknown masses and self-calibrations they are stronger.

Increasing the bin size to $\delta z^p=0.2$ but keeping $N_z=20$ (i) produces a coarser probe of cluster mass function but (ii) reduces the Poisson noise in the counts, therefore increasing the importance of sample variance and clustering self-calibration. Notice though that in all cases absolute errors increase with δz^p since subdividing the data can only help constraints.

If in addition to using coarser bins of $\delta z^p=0.2$ we simultaneously decrease the number of photo-z parameters to $N_z=10$ so as to still have one photo-z parameter per photo-z bin, the degradations in all cases become slightly better than in the fiducial model, although around slightly worse baselines. That shows that our results are relatively robust to the particular binning choice if we keep the number of photo-z parameters per bin of true redshift constant. In this case, coarser photo-z bins lose shape information on the redshift distribution but allows the fewer photo-z parameters to be better known by the same factor that they were reduced in number. Since the best achievable constraints are worse with such wider bins and the power of cluster counts surveys lies exactly in their ability to split the counts in a reasonable number of redshift and mass bins, photo-z bins much coarser than these are unlikely to be adopted in future cluster survey analyses if they are to be competitive dark energy probes.

E. Training Set Requirements

The photo-z requirements for a fixed dark energy degradation ultimately translate into requirements on the size of the calibration training set (with known redshifts), from which we infer the photo-z error parameters. With the assumption made here that the cluster photo-z errors have a Gaussian distribution, the uncertainties in the photo-z parameters $z^{\rm bias}(z_i)$ and $\sigma_z^2(z_i)$ in a given redshift bin i are related to the number $N_{\rm spec}(z_i)$ of spectroscopic training set calibrators in that bin by

$$\sigma(z^{\rm bias}(z_i)) \;=\; \sigma_z(z_i)\sqrt{\frac{1}{N_{\rm spec}(z_i)}}\,, \tag{30}$$

$$\sigma(\sigma_z^2(z_i)) \;=\; \sigma_z^2(z_i)\sqrt{\frac{2}{N_{\rm spec}(z_i)}}\,. \tag{31}$$

We are interested in the values of $N_{\rm spec}$ necessary in order not to degrade dark energy constraints appreciably. There are basically two ways to go about this question, which depend on the choice of the spectroscopic calibrators. The first case corresponds to choosing the calibrators to be clusters with at least one member galaxy whose spectroscopic redshift has been measured, in which case $N_{\rm spec}$ corresponds to the number of such spectroscopic clusters and $\sigma_z(z_i)$ is the cluster photo-z scatter in the

redshift bin. This choice is natural, but may suffer from the fact that a small number of such clusters are likely to be available in a given survey. The second choice then tries to compensate for that by including more objects in the calibration process. Since most clusters contain large numbers of red elliptical galaxies and optical cluster finder methods are typically tuned to find exactly such clusters, one can try to use not only the cluster spectroscopic redshifts, but the redshifts of all spectroscopic elliptical galaxies including field galaxies. Although this would make use of a much larger sample of objects, they would typically have a larger photo-z scatter and the assumption that all red galaxies (in the field and in clusters) share the same photo-z error properties would have to be checked. In any case, the first choice is general enough in the sense that we can think of the red galaxy sample as being used, not directly in the cluster photo-z parameters calibration, but in the estimation of these parameters. From that perspective, having a large spectroscopic sample of red galaxies helps calibrate the photo-z's of cluster member galaxies and decrease the cluster photo-z scatter, since each cluster member provides roughly an independent photo-z measurement of the cluster photo-z. Even though some cluster finding methods, such as those based on the SZ signal and weak lensing shear, do not preferentially detect clusters with large numbers of red galaxies, most future cluster surveys will have a spectroscopic follow-up of a sample of the detected clusters. For that reason, in the following analysis we will take the first choice of redshift calibrators, i.e. spectroscopic clusters.

Recall in Fig. 2 we considered fixed degradations in the dark energy equation of state w, given priors $\sigma(z^{\rm bias})$ and $\sigma(\sigma_z^2)$ which were *constant* in redshift. In that case, each value of d_w requires $\sigma(z^{\rm bias})$ and $\sigma(\sigma_z^2)$ to be lower than certain values, which in turn produce lower limits on $N_{\rm spec}(z_i)$. For illustrative purposes let us fix $d_w = 10\%$ and consider the fiducial model with counts information only, in which case Fig. 2 requires $\sigma(z^{\rm bias}) < 0.003$ and $\sqrt{\sigma(\sigma_z^2)} < 0.03$. The condition on $\sigma(z^{\rm bias})$, which is more stringent than the one on $\sigma(\sigma_z^2)$, requires the number of calibrators in bins of $\delta z_i = 0.1$ to be $N_{\rm spec}(z_i = 0.5) > 110$ and $N_{\rm spec}(z_i = 1.95) > 870$. However, all these numbers are excessively high due to our requirement of constant $\sigma(z^{\rm bias})$ and $\sigma(\sigma_z)$ in each bin, including the high redshift ones that have little impact on the dark energy constraints.

To remedy this problem, let us instead take $N_{\rm spec}$ to be a fixed fraction of the total number in a given bin

$$N_{\rm spec}(z_i) = a m_i \,. \tag{32}$$

We can then study the requirements on dark energy degradations as a function of a. We should keep in mind though that, observationally, it is even harder to obtain spectra for the few clusters at high redshifts compared to those (also few ones) at very low redshift, because at higher redshifts the 4000Å break of elliptical galaxies leaves the optical filter coverage. Therefore in practice a will probably be a decreasing function of redshift.

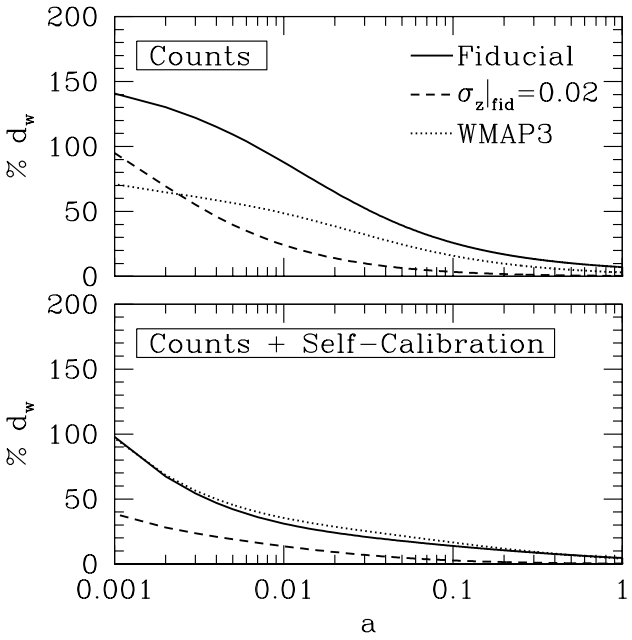

FIG. 8: Dark energy parameters degradation in the dark energy equation of state as a function of the fraction a of clusters with spectroscopic redshifts for the fiducial model, WMAP3 cosmology and photo-z scatter of $\sigma_z|_{\rm fid} = 0.02$, using counts information only and self-calibration.

In Fig. 8, we show the degradation d_w as a function of a in the fiducial model and also for the WMAP3 cosmology as well as the case with $\sigma_z|_{\rm fid} = 0.02$. Notice that even in the limit where all clusters have photo-z's ($a = 1$), because the number of these clusters is finite, we still have some degradation compared to the case where the photo-z parameters have zero uncertainties. Even though this *intrinsic* degradation can be as high as $\sim 10\%$, as shown in the top panel of Fig. 8, if a was actually equal to 1, one would not use photo-z's in the first place, since all objects would have perfect redshift measurements. Therefore actual degradations are smaller than those shown in Fig. 8 for very high values of a. Also, in practice only values of a that realize integer numbers of clusters are allowed. However, since we are considering a constant in redshift, we used continuous values of a, even those that give $N_{\rm spec} < 1$. Thus, actual degradations for very low values of a are larger than those shown in Fig. 8, especially for WMAP3.

Ignoring these caveats just mentioned, we see from the top panel in Fig. 8 that the WMAP3 case has a smaller degradation than the fiducial model when employing counts only, consistently with the results of §V D 1. Moreover reducing the photo-z scatter has an important impact on the w degradation as expected.

From the bottom panel of Fig. 8, we see that self-calibration tends to make the training size requirements smaller in most cases. Interestingly, d_w in both the fiducial model and the WMAP3 cosmology are nearly identical as a function of a. That happens because for fixed

values of $\sigma(z^{\rm bias}(z_i))$ and $\sigma(\sigma_z^2(z_i))$, whereas w degradations are typically weaker for WMAP3, the numbers m_i of existing clusters are smaller and consequently the number of spectroscopic calibrators are reduced by the same factor, making it harder to achieve these photo-z accuracies.

These results highlight the importance of having the best photo-z estimators available, which allow for the photo-z scatter to be as small as possible; this has a direct impact in reducing the required calibration set size. In the context of self-calibration, having spectroscopic redshifts for only $\sim 1\%$ of the clusters is enough to keep $d_w \lesssim 30\%$, whereas in the case of counts only, this spectroscopic sample needs to contain at least $\sim 8\%$ of the clusters. For a more stringent requirement of $d_w \lesssim 20\%$, with self-calibration it is necessary to have spectroscopic redshifts for $\sim 4\%$ of the clusters. Quantitatively, this requires $\sim$ 1300 spectroscopic clusters in the fiducial model and ~ 300 in the WMAP3 cosmology. Given that the training set size requirements for other cosmological probes such as weak lensing and baryon acoustic oscillations are on the order of hundreds of thousands, only a few percent of these galaxies need to be in clusters in order for those training sets to serve also as cluster calibration samples, without additional observational effort. Complementing the existing training sets with spectroscopic follow-up observations would then further improve dark energy constraints and allow for degradations at the percent level.

F. Caveats

There are a number of caveats associated with our results. We have taken a constant $M_{\rm th}^{\rm obs}$ whereas in reality we expect it to be cosmology and redshift dependent for a SZ survey like SPT (although less than in an X-ray survey [31]). Our constant fiducial $M_{\rm th}^{\rm obs}$ can be thought of as an effective mass threshold that produces the same number counts as the true threshold. If the effective mass threshold in a real survey deviates considerably from the one considered here, the baseline dark energy constraints will change, and so will the degradations with respect to this baseline. As discussed in §V, a change in $M_{\rm th}^{\rm obs}$ has an effect similar to a change in σ_8 or in the survey area, namely the change in the total cluster counts.

The variation of the observable-mass relation with cosmology may also open up parameter degeneracies. For our fiducial model we took the observable-mass distribution to be parametrized by $\ln M^{\rm bias}$ and $\sigma^2_{\ln M}$ with a fixed functional form in redshift. If this form instead mimicked the effect of a cosmological parameter, a degeneracy would appear. A complete treatment of these issues, which is beyond the scope of this work, would require the choice of a specific observable and extensive simulations to obtain the true parameter values and their distributions.

The potential impact of degeneracies can be assessed by considering the case where $\ln M^{\rm bias}$ and $\sigma^2_{\ln M}$ are allowed to be arbitrary functions of redshift (§V D). In this case the baseline dark energy constraints degrade by up to 80% relative to the fiducial model. Degradations on top of that due to uncertainties in $z^{\rm bias}$ and σ_z^2 become weaker and stronger respectively.

If one further includes an arbitrary mass dependence of these parameters, the techniques explored here are not sufficient to provide a good degree of self-calibration, even with perfect redshifts. Our results would still be valid as long as trends in mass are well-known close to the mass threshold [7]. Recent simulations [22, 23, 24] suggest that observable-mass relations can actually be parametrized with scaling relations involving few parameters as assumed here. Since our main purpose here is to illustrate the *relative* degradation of dark energy constraints due to photo-z errors, the range of models considered here should suffice.

Finally, we assumed the photo-z error parameters to follow a Gaussian distribution and depend on redshift but not mass. This assumption does not hold for field galaxies binned only in redshift due to the mixing of various galaxy types. Even though we expect Gaussian errors to be a good approximation for clusters, which have mostly red elliptical galaxies and lower photo-z scatter, possible non-Gaussian features induced by membership contamination may require proper modeling.

The photo-z parameters, in particular the photo-z scatter is expected to have some mass dependence. More massive clusters have more galaxies to average over when computing the cluster photo-z, allowing the photo-z scatter to decrease. We envision that the redshift/mass dependence of photo-z parameters can be modeled from mock catalogs and cast in simple scaling relations, likely depending on the particular cluster finder/survey. In the lack of any specific modeling, we chose to keep the redshift dependence general and ignore the mass dependence of the photo-z parameters. Lastly, we did not take into account possible errors in the theoretical cluster-mass function, which might introduce parameter biases or interact differently with photo-z errors.

VI. DISCUSSION

The use of cluster abundance as a competitive cosmological probe requires strict knowledge of both the cluster observable-mass relations and photo-z's. Self-calibration techniques help break degeneracies between cosmology and cluster masses and, at the same time, decrease redshift knowledge requirements. When external mass calibrations are available, self-calibration may become even more important, assisting monitor redshifts and providing interesting consistency checks. Conversely, good photo-z knowledge is required in order to extract optimal constraints from self-calibration methods.

We studied the effect of photo-z uncertainties in dark energy constraints assuming a fiducial model with sur-

vey specifications similar to the SPT, a constant mass threshold $M_{\rm th}^{\rm obs}$, a mass bias $\ln M^{\rm bias}$ parametrized by a power law in redshift, a mass variance $\sigma^2_{\ln M}$ with a cubic redshift evolution and photo-z parameters assumed to be general functions of redshift but not mass.

For this fiducial model it will be necessary to have priors of $\sigma(z^{\rm bias}) \lesssim 0.003$ and $\sqrt{\sigma(\sigma_z^2)} \lesssim 0.03$ in the case of perfect masses and counts information in order not to degrade dark energy constraints by more than $\sim 10\%$. In the case of self-calibration of the observable-mass relation, these priors uncertainties should be kept at $\sigma(z^{\rm bias}) \lesssim 0.004$ and $\sqrt{\sigma(\sigma_z^2)} \lesssim 0.04$. These requirements become weaker/stronger if we increase/decrease the number of nuisance parameters describing masses and redshifts or if we consider less/more ambitious surveys or cosmologies yielding less/more clusters.

In order to achieve these requirements, it is important not only to use the best general photo-z techniques, but also to understand the cluster finding selection functions and contamination fractions; otherwise even if the photo-z methods work well for field galaxies, the cluster redshifts and masses might be misestimated. Large and representative training sets help decrease the redshift uncertainties and keep the dark energy constraints close to their baseline values and also help self-calibration be more effective. From the self-calibration perspective, simulations play a very important role. Self-calibration techniques are more effective when we can parametrize the observable-mass relation with a small number of parameters, typically with simple scaling relations. Simulations do not need to determine exact values of these parameters, but only provide a good confidence that these simple relations are stable to theoretical uncertainties and have relatively small theoretical scatter. If that is the case one can extract these parameter values from self-calibration methods, which use information that naturally comes in surveys without requiring additional observational efforts.

Photo-z methods are expected to be ever improving during the evolution of ongoing and future surveys such as the Panoramic Survey Telescope and Rapid Response System (PanSTARRS) [32], the SPT [29], the Dark Energy Survey (DES) [33], the Supernova Acceleration Probe (SNAP) [34] and the Large Synoptic Survey Telescope (LSST) [35]. There are good prospects for the existence of large and representative training sets that will allow these surveys to be reasonably well calibrated. Likewise we expect simulations to improve our knowledge of the dark matter halo mass-functions and of the various observable-mass relations. External calibrations from weak lensing are likely to also play an important role in mass determinations. Finally, self-calibration methods can further help reduce requirements and provide important consistency checks that theoretical assumptions have been or not realized in the observations. All these aspects will be important and complementary in consistent cosmological analyses of future cluster surveys.

Acknowledgments: We thank Carlos Cunha, Josh Frieman, Huan Lin, Zhaoming Ma, and Hiroaki Oyaizu for useful discussions. This work was supported by the DOE and the KICP under NSF PHY-0114422. WH was additionally supported by the David and Lucile Packard Foundation.

APPENDIX A: WINDOW FUNCTION

Recall we used spherical coordinates $\mathbf{x} = (r, \theta, \phi)$ to parametrize the position vector describing the window volume element such that $d^3x = r^2 d\Omega dr$ with $d\Omega = \sin\theta d\theta d\phi$. The cell defines a solid angle given by $\Delta\Omega = \pi\theta_s^2$ in the small angle approximation. For convenience, we will also use cylindrical coordinates to parametrize the same vector $\mathbf{x} = (r, \rho, \phi)$, where $r(z)$ is still the angular diameter distance to redshift z and now the perpendicular coordinates (ρ, ϕ) parametrize the angular extension of the window. In these coordinates we have $d^3x = \rho d\rho d\phi dr$ and the cell defines a extension of $\rho_s = r\theta_s$. We split the total window function into $W_i(\mathbf{x}) = W_{\perp i}^{\rm th}(\rho, \phi) F_i(z)$. Here and below the superscript "th" denotes a top hat function whose value is unity within the pixel and zero outside of the pixel.

The volume-normalized Fourier transform of the window is given by

$$\begin{aligned} W_i(\mathbf{k}) &= \frac{1}{V_i}\int d^3x e^{i\mathbf{k}.\mathbf{x}} W_i(\mathbf{x}) \\ &= \frac{1}{V_i} W_{\perp i}^{\rm th}(\mathbf{k}_\perp) W_{\parallel i}(k_\parallel)\,, \end{aligned} \tag{A1}$$

where the window volume is

$$V_i \equiv \int d^3x W_i(\mathbf{x}) = \Delta\Omega \int dr r^2 F_i(z) \tag{A2}$$

and we defined

$$W_{\perp i}^{\rm th}(\mathbf{k}_\perp) \equiv \int d\rho d\phi \rho e^{ik_\perp \rho\cos\phi} W_{\perp i}^{\rm th}(\rho, \phi)\,, \tag{A3}$$

$$W_{\parallel i}(k_\parallel) \equiv \int dr e^{ik_\parallel r} F_i(z)\,. \tag{A4}$$

Note that the normalized Fourier window $W_i(\mathbf{k}) \to 1$ as $\mathbf{k} \to 0$.

Similarly, in the case of a top hat total window we would have

$$W_i^{\rm th}(\mathbf{k}) = \frac{1}{V_i^{\rm th}} W_{\perp i}^{\rm th}(\mathbf{k}_\perp) W_{\parallel i}^{\rm th}(k_\parallel)\,, \tag{A5}$$

with

$$V_i^{\rm th} \equiv \int d^3x W_i^{\rm th}(\mathbf{x}) = \Delta\Omega \int dr r^2 W_{\parallel i}^{\rm th}(r)\,. \tag{A6}$$

From Eqs. (A1) and (A5) we may write

$$\frac{W_i(\mathbf{k})}{W_i^{\rm th}(\mathbf{k})} = \frac{V_i^{\rm th}}{V_i} \frac{W_{\parallel i}(k_\parallel)}{W_{\parallel i}^{\rm th}(k_\parallel)}\,, \tag{A7}$$

and we can rewrite Eq. (A4) as

$$W_{\parallel i}(k_\parallel) \;=\; \int \frac{dz}{H(z)} e^{ik_\parallel r(z)} F_i(z)\,. \qquad \text{(A8)}$$

We will assume that $H(z)$ does not change appreciably in the photo-z bin and, because $F_i(z)$ quickly drops outside the bin, the values of r that contribute to the integral are restricted to the range $r = r_i \pm \delta r_i/2$ with $\delta r_i \approx \delta z_i^p/H_i$ and $H_i \equiv H(z_i^p)$, so that

$$W_{\parallel i}(k_\parallel) \approx \frac{1}{H_i}\int dz e^{ik_\parallel z/H_i} F_i(z) = \frac{F_i(k_{z,i})}{H_i}\,, \qquad \text{(A9)}$$

where we defined $k_{z,i} = k_\parallel/H_i$. Note that $F_i(z)$ can be expressed as a convolution of the Gaussian selection with a top hat window in redshift

$$F_i(z) = \int dz^{\rm phot} W_{\parallel i}^{\rm th}(z^{\rm phot}) p(z^{\rm phot}|z)\,. \qquad \text{(A10)}$$

The convolution theorem gives $F_i(k_{z,i}) = W_{\parallel i}^{\rm th}(k_{z,i})p(k_{z,i})$ so that Eq. (A9) becomes

$$W_{\parallel i}(k_\parallel) = \frac{W_{\parallel i}^{\rm th}(k_{z,i})p(k_{z,i})}{H_i}\,. \qquad \text{(A11)}$$

By a similar argument that led to Eq. (A9) we have that $W_{\parallel i}^{\rm th}(k_{z,i}) \approx H_i W_{\parallel i}^{\rm th}(k_\parallel)$ and Eq. (A7) becomes

$$\frac{W_i(\mathbf{k})}{W_i^{\rm th}(\mathbf{k})} = \frac{V_i^{\rm th}}{V_i} p(k_{z,i})\,. \qquad \text{(A12)}$$

In the limit where $r(z)$ and the photo-z parameters $z^{\rm bias}$ and σ_z^2 do not change appreciably inside the photo-z bin, the window volumes in the absence ($V_i^{\rm th}$) and presence of photo-z errors (V_i) roughly coincide $V_i \approx V_i^{\rm th} \propto r_i^2 \delta r_i$, i.e. the photo-z errors distort the volume element but do not change its value. Therefore we have

$$W_i(\mathbf{k}) = W_i^{\rm th}(\mathbf{k}) p(k_{z,i}). \qquad \text{(A13)}$$

The Fourier transform of the top hat window is [26]

$$W_i^{\rm th}(\mathbf{k}) \;=\; 2e^{ik_\parallel r_i}\frac{\sin(k_\parallel \delta r_i/2)}{k_\parallel \delta r_i/2}\frac{J_1(k_\perp r_i\theta_s)}{k_\perp r_i \theta_s} \qquad \text{(A14)}$$

and for the Gaussian distribution we have

$$p(k_{z,i}) \;=\; e^{ik_{z,i}z_i^{\rm bias}} e^{-\sigma_{z,i}^2 k_{z,i}^2/2}. \qquad \text{(A15)}$$

Combining these results, we obtain

$$W_i(\mathbf{k}) \;=\; 2\exp\left[ik_\parallel\left(r_i + \frac{z_i^{\rm bias}}{H_i}\right)\right]\exp\left(-\frac{\sigma_{z,i}^2 k_\parallel^2}{2H_i^2}\right) \frac{\sin(k_\parallel \delta r_i/2)}{k_\parallel \delta r_i/2}\frac{J_1(k_\perp r_i\theta_s)}{k_\perp r_i\theta_s}$$

for the window function.

[1] J.-Y. Tang, J. Weller, and A. Zablocki (2006), astro-ph/0609028.
[2] S. Wang, Z. Haiman, W. Hu, J. Khoury, and M. May, Phys. Rev. Lett. **95**, 011302 (2005), astro-ph/0505390.
[3] M. Gladders et al., Astrophys. J. **655**, 128 (2007), arXiv:astro-ph/0603588.
[4] E. Rozo et al., ArXiv Astrophysics e-prints (2007), astro-ph/0703571.
[5] S. Majumdar and J. Mohr, Astrophys. J. **585**, 603 (2003), astro-ph/0208002.
[6] M. Lima and W. Hu, Phys. Rev. D **70**, 043504 (2004), astro-ph/0401559.
[7] M. Lima and W. Hu, Phys. Rev. D **72**, 043006 (2005), astro-ph/0503363.
[8] W. Hu, Phys. Rev. D **67**, 081304 (2003), astro-ph/0301416.
[9] J. D. Younger, Z. Haiman, G. L. Bryan, and S. Wang (2006), astro-ph/0605204.
[10] C. Cunha, H. Oyaizu, M. Lima, H. Lin, and J. Frieman, in prep. (2007).
[11] H. Oyaizu, M. Lima, C. E. Cunha, H. Lin, J. Frieman, and E. S. Sheldon, ArXiv e-prints **708** (2007), 0708.0030.
[12] M. Gladders and H. Yee, Astron. J. **120**, 2148 (2000), astro-ph/0004092.
[13] B. Koester et al., Astrophys. J. **660**, 221 (2007), arXiv:astro-ph/0701268.
[14] D. Trevese, M. Castellano, A. Fontana, and E. Giallongo, ArXiv Astrophysics e-prints (2006), astro-ph/0611895.
[15] F. Dong, E. Pierpaoli, J. E. Gunn, and R. H. Wechsler, ArXiv e-prints **709** (2007), 0709.0759.
[16] D. Huterer, A. Kim, L. M. Krauss, and T. Broderick, Astrophys. J. **615**, 595 (2004), astro-ph/0402002.
[17] H. Zhan and L. Knox, Astrophys. J. **644**, 663 (2006), astro-ph/0509260.
[18] H. Zhan, JCAP **0608**, 008 (2006), astro-ph/0605696.
[19] D. Huterer, M. Takada, G. Bernstein, and B. Jain, Mon. Not. R. Astron. Soc. **366**, 101 (2006), astro-ph/0506030.
[20] Z. Ma, W. Hu, and D. Huterer, Astrophys. J. **636**, 21 (2006), astro-ph/0506614.
[21] A. Jenkins et al., Mon. Not. R. Astron. Soc. **321**, 372 (2001).
[22] A. V. Kravtsov, A. Vikhlinin, and D. Nagai, Astrophys. J. **650**, 128 (2006), arXiv:astro-ph/0603205.
[23] D. Nagai, Astrophys. J. **650**, 538 (2006), arXiv:astro-ph/0512208.
[24] T. B. O'Hara, J. J. Mohr, J. J. Bialek, and A. E. Evrard, Astrophys. J. **639**, 64 (2006), arXiv:astro-ph/0510064.
[25] R. Sheth and B. Tormen, Mon. Not. R. Astron. Soc. **308**, 119 (1999).
[26] W. Hu and A. Kravtsov, Astrophys. J. **584**, 702 (2003),

astro-ph/0203169.
[27] G. Holder, Z. Haiman, and J. Mohr, Astrophys. J. Lett. **560**, 111 (2001).
[28] W. Hu and J. D. Cohn, Phys. Rev. D **73**, 067301 (2006), astro-ph/0602147.
[29] J. Ruhl et al. (2004), vol. 5498 of *Proc. of the SPIE*, pp. 11–29.
[30] W. Hu and B. Jain, Phys. Rev. D **70**, 043009 (2004), astro-ph/0312395.
[31] Z. Haiman, J. Mohr, and G. Holder, Astrophys. J. **553**, 545 (2001), astro-ph/0002336.
[32] N. Kaiser et al. (2002), vol. 4836 of *Proc. of the SPIE*, p. 154.
[33] The Dark Energy Survey Collaboration, ArXiv Astrophysics e-prints (2005), astro-ph/0510346.
[34] G. Aldering, New Astronomy Review **49**, 346 (2005), arXiv:astro-ph/0507426.
[35] J. A. Tyson, D. M. Wittman, J. F. Hennawi, and D. N. Spergel, Nuclear Physics B Proceedings Supplements **124**, 21 (2003), arXiv:astro-ph/0209632.